GRAIL CONSTRAINTS ON THE VERTICAL DENSITY STRUCTURE OF THE LUNAR CRUST. Jonathan Besserer, Francis Nimmo, *Dept. Earth & Planetary Sciences, U.C. Santa Cruz, Santa Cruz CA 95064, USA (jbessere@ucsc.edu)*, Mark A. Wieczorek, *Institut de Physique du Globe de Paris, Sorbonne Paris Cité, Université Paris Diderot, 75205 Paris, France*, Renee C. Weber, *NASA Marshall Space Flight Center, Huntsville AL 35805, USA*, Walter S. Kiefer, Patrick J. McGovern, *Center for Lunar Science and Exploration, Lunar and Planetary Institute, Houston TX 77058, USA*, David E. Smith, Maria T. Zuber, *Department of Earth, Atmospheric and Planetary Sciences, Massachusetts Institute of Technology, Cambridge MA 02139, USA*.

Introduction: The bulk density of the porous lunar crust has been mapped using high-resolution gravity provided by the Gravity Recovery and Interior Laboratory (GRAIL) mission [1, 2, 3]. However, the vertical structure of the crust, which is key to understanding its thermal [4, 5] and seismic [6] characteristics, and its origin and subsequent modification, is currently poorly known [2, 3]. Here, we analyze GRAIL data using an admittance approach to determine the vertical density structure of the lunar crust.

Approach: We used spherical harmonic coefficients of the Moon's gravity [1], topography [9], and topography-induced gravity [2] fields up to spherical harmonic degree $\ell = 550$. The gravity data were derived from the GRAIL nominal and extended missions' tracking data; the topography data were derived from the principal axis referenced Lunar Orbiter Laser Altimeter (LOLA) data [9]. A localized, multitaper spherical harmonic analysis was performed [7, 8] at each position on a grid of 400 nodes distributed in a quasi-equal area fashion [2], yielding a node spacing of $\sim$290 km. Optimal windows (tapers) of large spectral bandwith ($L = 58$) were used to localize the gravity and topography-induced gravity data in spherical cap regions 15° in radius. The resulting fields were expanded in spherical harmonics, from which the effective density ρ_{eff} (which compares the observed gravity to the predicted gravity) as a function of ℓ was calculated:

$$\rho_{\text{eff}}(\ell) = \frac{S_{gb}(\ell)}{S_{bb}(\ell)}, \quad (1)$$

where g and b refer to the observed gravity and to the gravity predicted from topography assuming unit density, respectively, and S_{fg} is the cross-power spectrum of two functions f and g on the sphere.

The resulting localized effective density spectra typically show an increase in density with decreasing ℓ (e.g., Figure 1), implying that density increases with depth [3, 10]. These spectra were fit to two kinds of theoretical spectra assuming either a linear or an exponential density profile in the crust. The fits were performed for the high-degree part of the data ($250 \leq \ell \leq 550$), in order to avoid the effects of flexure and/or crustal thickness variations at lower degrees. Our method is therefore mostly sensitive to the shallow density structure of the crust (typically depths $z <$ 10-15 km). The best-fit parameters describing the theoretical spectra were derived using a grid search.

Linear density model: Figure 2 shows the spatial distribution of the best-fitting linear density gradient a. The mare regions exhibit high surface densities and a distinct decrease in density with depth, as expected if (high density) mare basalts overlie (lower density) anorthositic crust. The linear model can thus discriminate between mare and non-mare regions, and also provides a potential way of identifying regions of buried (crypto-) mare [11]. However, some mare are not detected, probably because these features are too small, either laterally or vertically. By constrast, most of the farside is characterized by an increase in density with depth, with typical gradients of 10-30 kg m^{-3} km^{-1}. The Apollo 12 & 14 landing sites lie in a region that resembles the farside in terms of vertical density structure. The Apollo 15 & 17 sites, where the only lunar heat flow measurements were carried out [5], lie in typical mare-bearing regions with negative values of a. The general density increase with depth that characterizes the farside highlands presumably reflects a decrease in porosity with depth [3, 10].

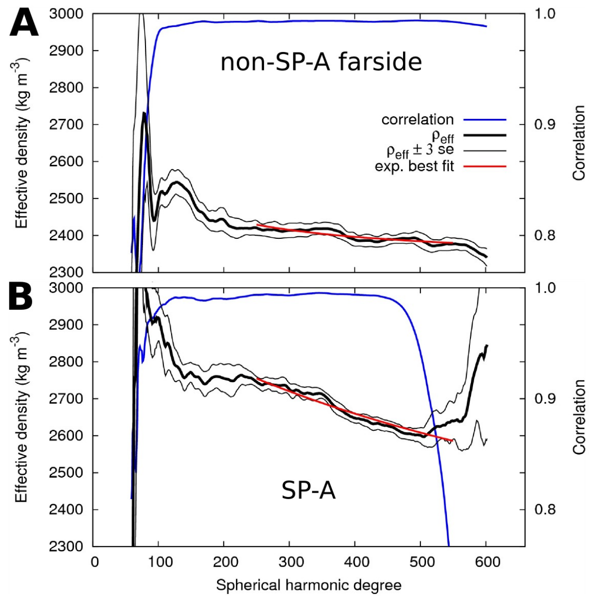

Figure 1: Example of observed and modeled effective density spectra for two endmember regions on the farside. Corresponding regions of interest are located (cf. Figs. 2-3) inside (B) and external to (A) the South Pole-Aitken (SP-A) basin region. Note the general lower effective density of the non-SP-A spectrum. Data are displayed over the degree range $L < \ell < 660 - L$, with $L = 58$ the multitaper window's spectral bandwidth. The various lines depict the observed effective density spectra (thick black line), with associated ±3 standard error levels, the best-fit theoretical spectra assuming an exponentially varying density (red), and the local correlation (blue).

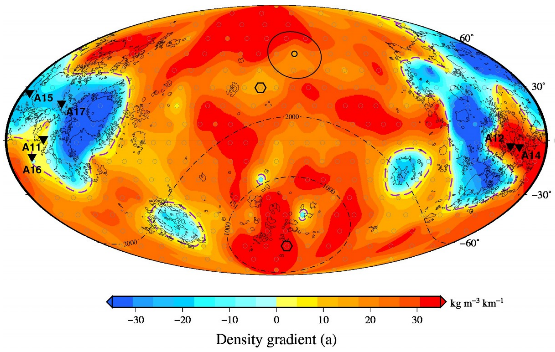

Figure 2: Best-fitting shallow crustal density gradient a inferred from a linear model profile [$\rho(z) = \rho_{\text{surf}} + a\,z$]. Triangles depict the location of the six Apollo landing sites. The two dash-dotted lines indicate equidistant points at 1000 and 2000 km from the center of the SP-A impact basin. Thin lines outline the maria. The thick line shows the radial extent (15°) of the employed localization window. The two hexagons indicate the locations depicted in Fig. 1. The purple dashed lines depict the limit between regions with $a > 5$ kg m^{-3} km^{-1} and with $a < 5$ kg m^{-3} km^{-1}. Data are presented in an equatorial view, centered on the farside – Mollweide equal area projection.

Exponential density model: We now focus on regions characterized by a density increase with depth, in particular the farside and the SP-A basin region. In the following, regions with gradients less than +5 kg m^{-3} km^{-1} (our finite grid-search step) were excluded (purple dashed line in Figure 2). We assume a more realistic density distribution consisting of an exponential profile given by $\rho(z) = \rho_{\text{surf}} + \Delta\rho\,(1 - e^{-z/d})$, where d is an e-folding depth and $\Delta\rho$ is the total density contrast across the crust. We assume that $\rho_0 = \rho_{\text{surf}} + \Delta\rho$ is that of the intact surface rock (i.e. grain) density. For each location, the local, window-averaged value of ρ_0 was calculated from a grain density model [12], although our results did not change if a single, constant value for ρ_0 was used. For the farside highlands as a whole, the best-fit density profile characteristics are: $d = 10 \pm 2$ km and $\rho_{\text{surf}} = 2261^{+34}_{-42}$ kg m^{-3}, corresponding to a typical surface porosity of 21-24 % (the average grain density being 2917 kg m^{-3}); the equivalent density gradient with a linear model is $a \approx 30$ kg m^{-3} km^{-1}. Such high inferred surface porosity values are compatible with Apollo samples and lunar meteorites [13]. Figure 3 shows the spatial distribution of the e-folding lengthscale d. The most striking result is that the SP-A impact basin region has a significantly shallower low-density (porous) layer than the rest of the farside, with $d =$ 5-10 km, instead of 15-25 km.

The SP-A region appears to possess a shallower porous layer than the rest of the farside. This could be the result of: impact-induced removal (excavation) of pre-existing fractured material; annealing of pre-existing fractures [2] within SP-A; generation of a thick, pore-free impact melt sheet [15] within SP-A; intrusive processes; redistribution of thick (porous) SP-A ejecta deposits over the rest of the farside; or a combination of these factors. The SP-A impact may have caused widespread deposition of up to a few kilometers of ejecta [16, 17].

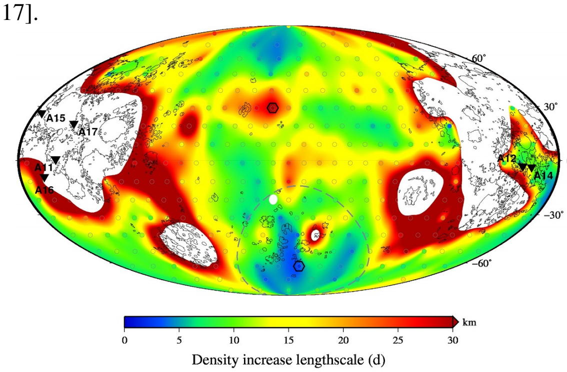

Figure 3: Spatial distribution of the best-fitting lengthscale d for a model with an exponential density profile [$\rho(z) = \rho_{\text{surf}} + \Delta\rho\,(1 - e^{-z/d})$]. General image format is the same as in Fig. 2. The masked (white) areas corresponds to $a < 5$ kg m^{-3} km^{-1} in Fig. 2. The gray, dashed line corresponds to the best-fit ellipse (outer topography [14]) for SP-A.

Conclusion: Mare regions are characterized by a distinct decrease in density with depth, while the farside is characterized by an increase in density with depth at an average rate of $\sim$30 kg m^{-3} km^{-1} and typical surface porosities of 20%. The Apollo 12 & 14 landing site region has a similar density structure to the farside, permitting a comparison with seismic velocity profiles [18, 19]. The SP-A impact basin region appears distinct with a near-surface low-density (porous) layer 2-3 times shallower than the rest of the farside. This result suggests that redistribution of material during the large SP-A impact likely played a major role in sculpting the lunar crust. Mapping the spatial distribution of shallow porosity, as we have attempted here, will allow comparison with other data sets (e.g., seismic velocities, surface composition).

References: [1] Zuber M.T. et al. (2013), *Science 339,* 668-671. [2] Wieczorek M.A. et al. (2013), *Science 339,* 671-675. [3] Han S.-C. (2013), *J. Geophys. Res. 118,* 2323-2337. [4] Rasmussen K.L. and Warren P.H. (1985), *Nature 313,* 121-124. [5] Langseth M.G. et al. (1976), *Lun. Planet. Sci. Conf. VII,* 3143-3171. [6] Lognonne P. et al. (2003), *Earth Planet. Sci. Lett. 211,* 27-44. [7] Wieczorek M.A. and Simons F.J. (2005), *Geophys. J. Internat. 162,* 655-675. [8] Wieczorek M.A. and Simons F.J. (2007), *J. Fourier Anal. Appl. 13,* 665-692. [9] Smith D.E. et al. (2010), *Geophys. Res. Lett. 37,* 18204. [10] Wieczorek M.A. et al. (2013), *Lun. Planet. Sci. Conf. XLIV,* 1719. [11] Antonenko I. et al. (1995), *Earth Moon Planets 69,* 141-172. [12] Huang Q. and Wieczorek M.A. (2012), *J. Geophys. Res. 117,* E05003. [13] Kiefer W.S. et al. (2012), *Geophys. Res. Lett. 39,* 7201. [14] Garrick-Bethell I. and Zuber M.T. (2009), *Icarus 204,* 399-408. [15] Potter R.W.K. et al. (2012), *Icarus 220,* 730-743. [16] Petro N.E. and Pieters C.M. (2008), *Meteor. Planet. Sci. 43,* 1517-1529. [17] Wieczorek M.A. et al. (2012), *Science 335,* 1212-1215. [18] Wieczorek M.A. et al. (2006), *Rev. Mineral. Geochem. 60,* 221-364. [19] Khan A. et al. (2013), *Tectonophys. 609,* 331-352.